CHAPTER 3

MELT SPINNING STUDIES ON A MODEL POLYESTER : POLY(ε-CAPROLACTONE)

3.1 Introduction

At the outset of this project, it was decided that preliminary melt spinning trials needed to be carried out on a model polyester in order to evaluate the effects of some of the processing variables involved. This was considered necessary because the speciality polyesters which were to be the main subject of study in this research could only be synthesized in relatively small amounts (<50 g) at a time with inevitable variations from batch to batch. Therefore, a model polyester, commercially available and with similar properties, was required, The most obvious possibilities were poly(ethylene terephthalate), PET, and poly(ε-caprolactone), PCL.

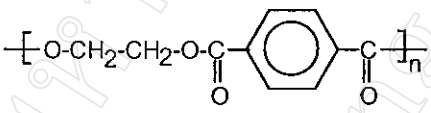

poly(ethylene terephthalate)

PET

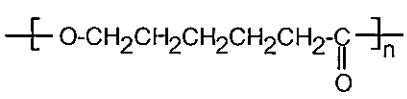

poly(ε-caprolactone)

PCL

After conducting melt spinning trials on both of these polyesters using the apparatus described in the previous chapter, it was decided that PCL would be a more appropriate model polymer for the following reasons:

(1) PCL is very easy to melt spin due to its low melting range and wide processing window. In contrast, PET is a difficult polymer to melt spin due to its high melting range and narrow processing window.

(2) In common with the speciality polyesters to be synthesized in this project, PCL is an aliphatic main chain polyester whereas the PET main chain contains an aromatic ring.

(3) The speciality polymers to be synthesized here also contain caprolactone (CL) units in either their copolymer or terpolymer structures.

Consequently, due to PCL's greater similarity to the polymers which are to form the subject of this study, both in terms of its chemical structure and physical properties, it is likely to have a more similar rheology than PET and therefore be more appropriate as a model polymer for melt spinning. It should also be noted here that PCL is a biomedical polymer in its own right. This is also a plus factor in its choice as a model polymer. Some of its properties and biomedical applications are described in the following section.

3.2 Poly(ε-caprolactone)

Poly(ε-caprolactone), PCL, or simply polycaprolactone as it usually referred to, is a synthetic biodegradable aliphatic polyester which has attracted considerable research attention in recent years, notably in the specialist biomedical areas of controlled-release drug delivery systems, absorbable surgical sutures and nerve guides, and 3-dimensional (3-D) scaffolds for use in tissue engineering [35-37]. PCL is manufactured commercially via the ring-opening polymerization in bulk of ε-caprolactone, CL, using tin (II) bis(2-ethylhexanoate), commonly known as stannous octoate, $Sn(Oct)_2$, as a coordination-insertion catalyst at a temperature of, typically, 140-150 °C.

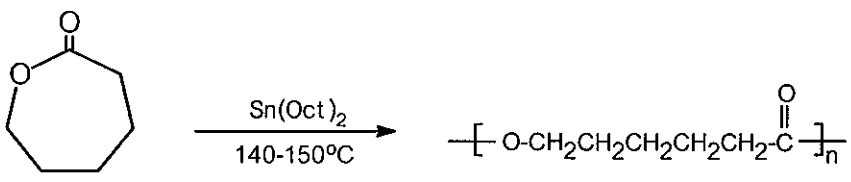

ε-caprolactone

CL

poly(ε-caprolactone)

PCL

As a commercial material, the main attractions of PCL are (1) its biodegradability, (2) its rather unique combination of polyolefin-like mechanical properties and polyester-like hydrolysability, (3) its compatibility with a wide range of other polymers, (4) its ease of melt processing due to its high thermal stability, and (5) its relatively low cost. On the other hand, its low melting point of around 60°C and its very slow rate of biodegradation in the human body (2-3 years) have tended to restrict its usage as a homopolymer. Consequently, PCL has been used more as a component in polymer blends or in the form of a copolymer. For example, in its biomedical applications, PCL has been blended with polymers such as cellulose propionate, cellulose acetate-butyrate, poly(lactic acid) and poly(lactic acid – *co* – glycolic acid) for use in long-term drug delivery systems [38-46]. As a copolymer for suture applications, ε-caprolactone monomer has been copolymerized with L-lactide [41,42] and, most successfully, with glycolide [43,44] to yield a segmented triblock copolymer which is marketed under the trade name of MONOCRYL® (Ethicon Inc.). Similarly, for use in absorbable nerve guides, ε-caprolactone has been copolymerized with DL-lactide[45] and trimethylene carbonate [46].

However, it is on PCL as a homopolymer that this part of the work focusses its attention and, in particular, on its melt spinning as a monofilament fibre. As mentioned previously, PCL by itself is most suited biomedically to the design of long-term implantable systems, the most well-known commercial example of which is CAPRONOR® (Research Triangle Institute, USA), a biodegradable capsular delivery system for contraceptive control developed by Pitt and Schindler [36,47]. In fibre form, PCL has also been investigated for use in drug delivery systems [48], as well as for "long-lasting" absorbable sutures [49], and, most recently, 3-D scaffolds for tissue engineering applications [50].

3.3 Polymer Characterisation

3.3.1 Experimental Methods

The PCL used in this work was a commercial product (Aldrich Chemical Co., Product No. 44,074-4) with a stated number-average molecular weight, $\overline{M}_n$, of approximately 80,000 (GPC). It was supplied in the form of white beads which were dried in a vacuum oven at 40°C for 24 hours before use in melt spinning. The polymer was not purified further by dissolution and reprecipitation since contact with organic solvents often leads to void formation in melt-spun fibres. Characterisation was carried out according to those polymer properties which were most relevant to its melt spinnability and solid-state morphology, namely: molecular weight, melting range, % crystallinity, crystallizability on cooling from the melt, thermal stability, and melt rheology.

Molecular weight determination was carried out by means of gel permeation chromatography (GPC) so that the $\overline{M}_n$ value could be compared directly with the supplier's own GPC $\overline{M}_n$ value of 80,000. The instrument used was a Waters 150-CV Gel Permeation Chromatograph employing both differential refractometer and viscometer detectors with universal calibration. Tetrahydrofuran (THF) was used as the solvent at a temperature of 30°C and flow-rate of 1 ml min^{-1}.

However, when it was found that there was considerable variance between the experimental and supplier's GPC $\overline{M}_n$ values, two additional molecular weight methods were also used, namely: (1) light scattering and (2) dilute-solution viscometry. Light scattering, an absolute method for the determination of the weight-average molecular weight, $\overline{M}_w$, was performed using a Malvern Instruments 4700 Light Scattering Photometer equipped with an argon ion laser (wavelength = 488 nm). Again, THF was used as the solvent but, in this case, at 35°C. Finally, dilute-solution viscometry was carried out using a Schott-Gerate AVS300 Automatic Viscosity Measuring System with benzene as the solvent at either 25°C or 30°C.

The polymer's melting range, % crystallinity, and crystallizability on cooling from the melt were characterized using a Perkin-Elmer DSC7 Differential Scanning Calorimeter, while its thermal stability was determined using a Perkin-Elmer TGA7 Thermogravimetric Analyzer.

Melt rheology and, in particular, the dependence of melt flow index on temperature was measured using a Davenport Melt Flow Indexer, Model 10.

3.3.2 Results

3.3.2.1 Molecular Weight Averages

The experimentally determined molecular weight averages, $\overline{M}_n$ and $\overline{M}_w$, are compared in Table 3.1 alongside the supplier's own $\overline{M}_n$ (GPC) value. In the case of dilute-solution viscometry, various Mark-Houwink Equations have appeared in the literature for PCL [36]. Of these, two of the most commonly reported are those shown in equations 3.1 and 3.2

$$[\eta] = 1.25 \times 10^{-4} \overline{M}_n^{0.82} \quad \text{(in benzene at 25°C) [51]} \quad (3.1)$$

$$[\eta] = 9.94 \times 10^{-5} \overline{M}_w^{0.82} \quad \text{(in benzene at 30°C) [52]} \quad (3.2)$$

where $[\eta]$ is the intrinsic viscosity in units of dl g^{-1}. These are the two equations that were used to calculate the viscometric $\overline{M}_n$ and $\overline{M}_w$ values in Table 3.1.

The GPC curve of the PCL beads is shown in Fig. 3.1 while the Zimm plot from light scattering is shown in Fig. 3.2. The $\overline{M}_w$ values of 52,000 and 45,100 respectively are in reasonably good agreement. Of the two, the latter should be the more reliable since light scattering is an absolute method of molecular weight determination. Similarly, the values of $\overline{M}_n$ = 32,700 and $\overline{M}_w$ = 46,300 from dilute-solution viscometry are consistent with the GPC and light scattering data and the corresponding viscosity-concentration double extrapolation plots are shown in Figs. 3.3 and 3.4.

As the results in Table 3.1 show, although the experimentally obtained values of $\overline{M}_n$ and $\overline{M}_w$ from the 3 different methods used are consistent with one another, the $\overline{M}_n$ values are significantly different from the supplier's $\overline{M}_n$ (GPC) value of 80,000. The reason for this is unclear but it may possibly be due to some hydrolytic degradation having occurred in the PCL beads since their manufacture. Whatever the reason may be, it illustrates the importance of not relying solely on the manufacturer's molecular weight data, especially where the polymer is moisture-sensitive and may unavoidably come into contact with air during storage.

Table 3.1 Comparison of the various molecular weight values obtained for the PCL beads used in this work.

Mol. Wt. Method	$\overline{M}_n$	$\overline{M}_w$	$\overline{M}_w/\overline{M}_n$
GPC			
Supplier's product data	80,000		
Experimentally found	26,500	52,000	1.99
Light Scattering		45,100 [a]	
Dilute-solution Viscometry	32,700 [b]	46,300 [c]	1.42

[a] as determined from a Zimm plot (Fig. 3.2)

[b] as calculated from equation 3.1

[c] as calculated form equation 3.2

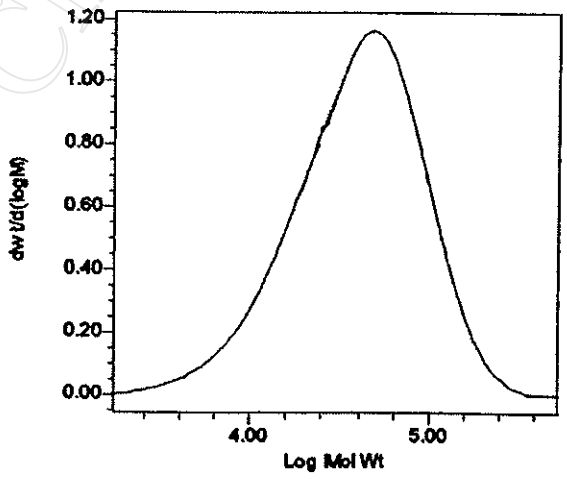

Fig. 3.1 GPC curve of the PCL beads.

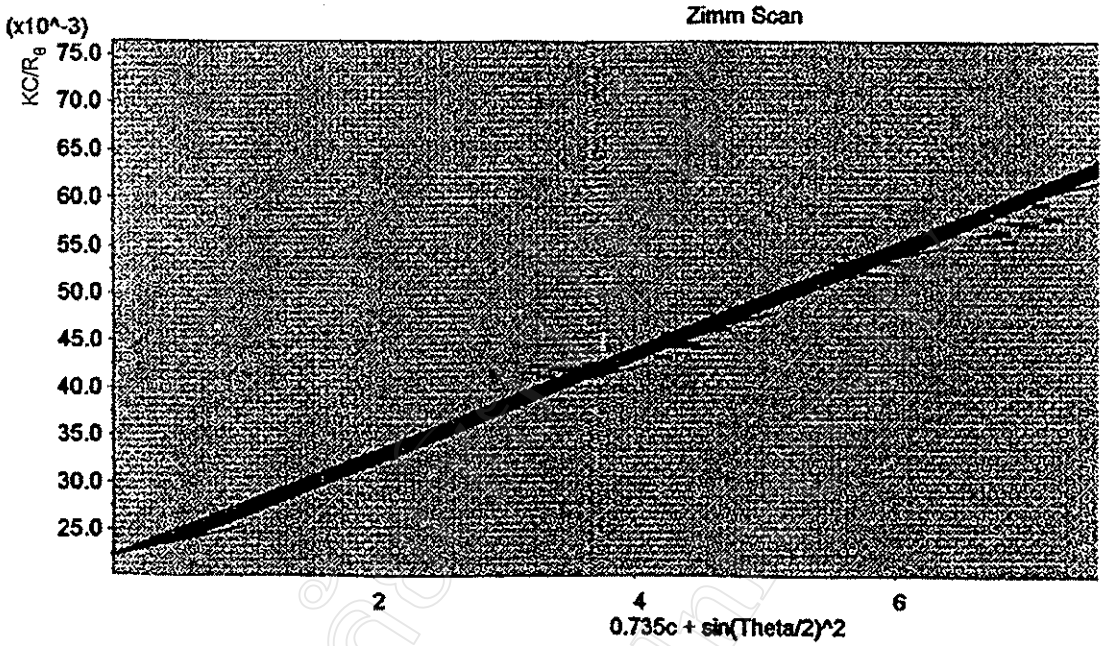

Fig 3.2 Zimm plot of the PCL beads from light scattering.

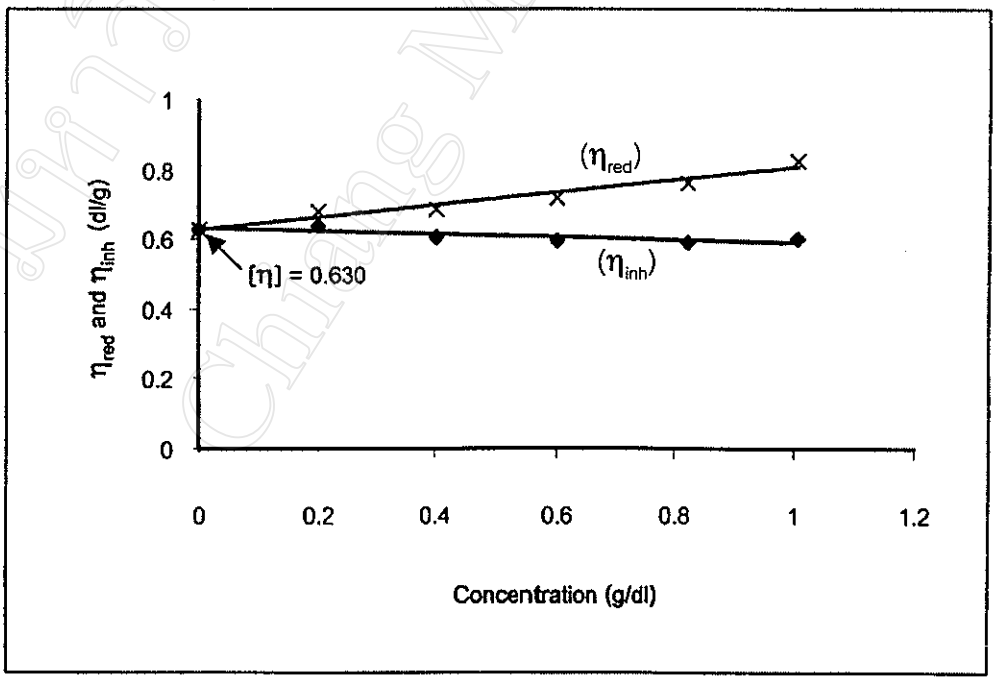

Fig. 3.3 Reduced (η_{red}) and inherent (η_{inh}) viscosity-concentration plots for the PCL beads in benzene as solvent at 25°C. (Gives $\overline{M}_n$ = 32,700 from equation 3.1)

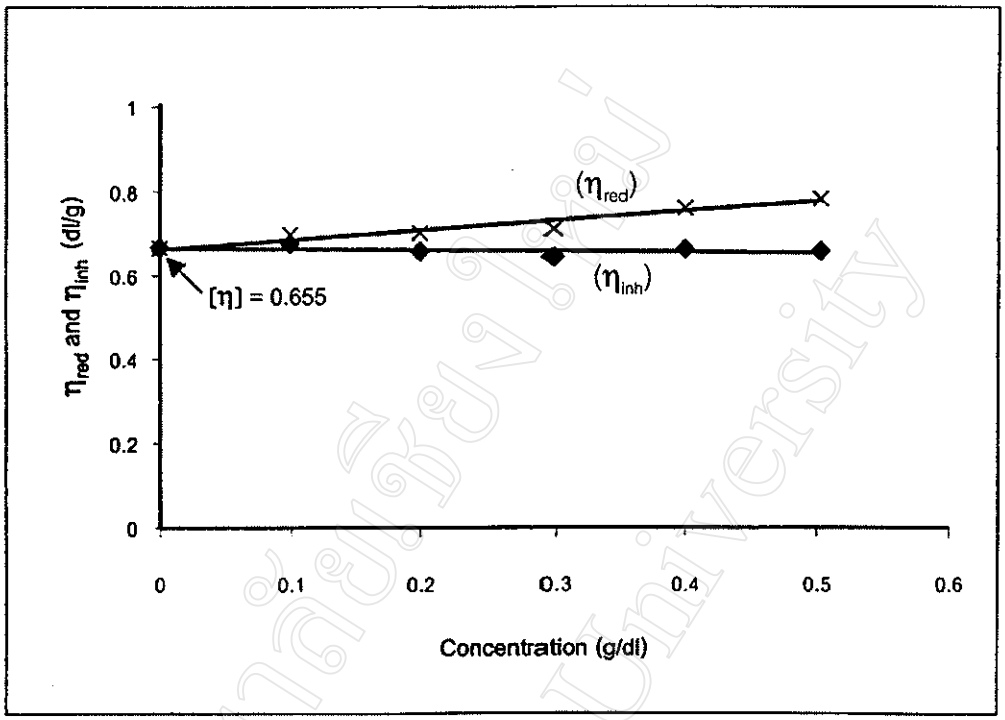

Fig. 3.4 Reduced (η_{red}) and inherent (η_{inh}) viscosity-concentration plots for the PCL beads in benzene as solvent at 30°C. (Gives $\overline{M}_w$ = 46,300 from equation 3.2)

3.3.2.2 Thermal Properties

The thermal properties of the PCL beads as supplied were characterized by a combination of differential scanning calorimetry (DSC) and thermogravimetry (TG). Their DSC heating and cooling curves are shown in Figs. 3.5 and 3.6 respectively. As the heating curve shows in Fig. 3.5(a), PCL is a semi-crystalline polymer of low melting range with a T_m (peak) of approximately 60°C. The polymer's % crystallinity can be determined from its heat of melting, ΔH_m , via the equation:

$$\% \text{ crystallinity} = (\Delta H_m \times 100) / \Delta H_m^* \qquad (3.3)$$

where ΔH_m^* is the heat of melting of a 100% crystalline sample. For PCL, ΔH_m^* has been reported in the literature as having a value of 139.5 J g^{-1} [53]. Thus, the experimental value of ΔH_m = 90.0 J g^{-1} from Fig. 3.5(a) yields a % crystallinity for the beads of 64%.

In addition to its crystallizability, the polymer's rate of crystallization on cooling from the melt is also an important consideration in melt spinning. As the DSC cooling curves in Fig. 3.6 show, PCL is able to crystallize quite easily on cooling from above its melting range down to ambient temperature (70 $\longrightarrow$ 20°C) at cooling rates of up to 10°C min^{-1}. This indicates that PCL is a relatively fast-crystallizing polymer, a property which can be ascribed to a high degree of chain flexibility and, because of its very low glass transition temperature (T_g = -60°C), a high degree of chain segmental mobility at ambient temperature.

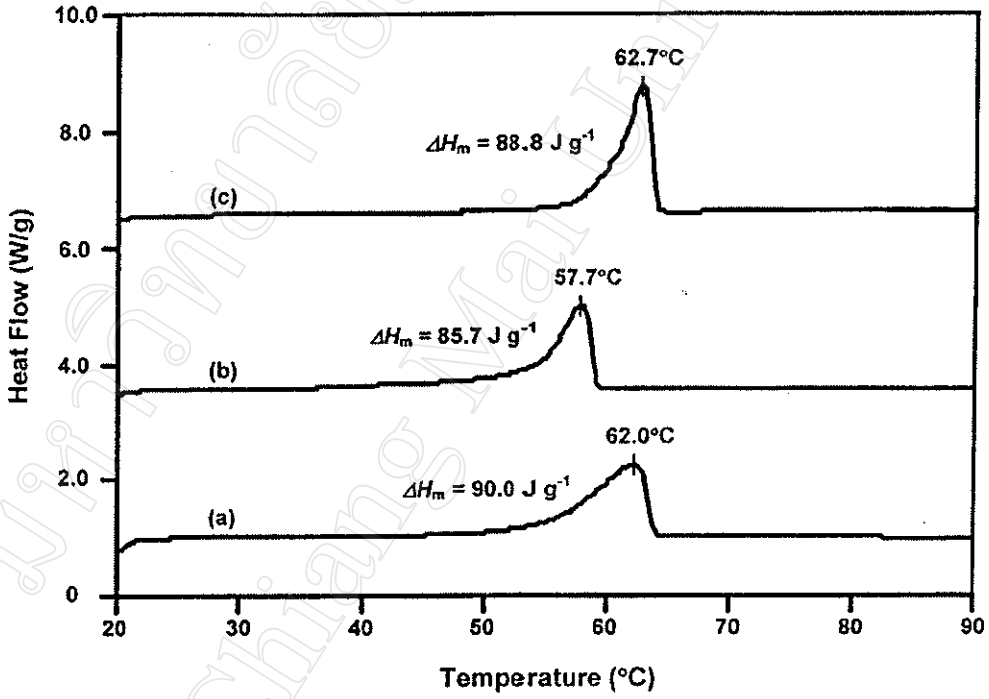

Fig. 3.5 DSC heating curves showing the melting peaks of (a) the PCL beads, (b) an as-spun fibre and (c) an off-line drawn (x25) fibre. (Heating rate = 5 °C/min)

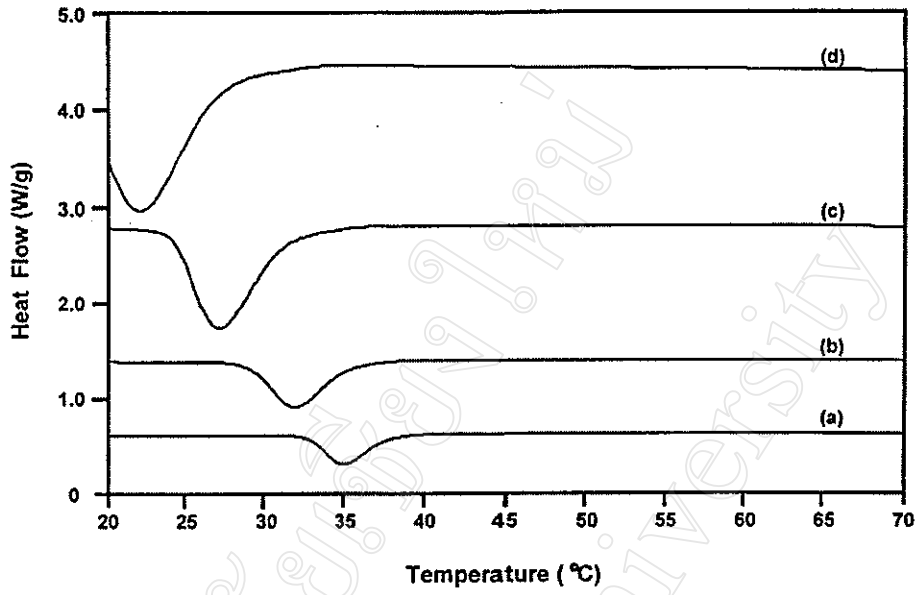

Fig. 3.6 DSC cooling curves showing the PCL crystallization peaks at cooling rates of (a) 1 °C min^{-1} (b) 2 °C min^{-1} (c) 5 °C min^{-1} and (d) 10 °C min^{-1}

On comparing the curves in Fig. 3.6, it appears that the crystallization exotherm (∝ peak area) increases with increasing cooling rate, contrary to expectation. In fact, this is misleading since the peak areas cannot be compared visually because the curves are not normalized according to scanning rate. When the individual heats of crystallization, ΔH_c , are computed for each curve and then compared, it is found that each cooling rate gives a very similar value of ΔH_c in the range of 55-60 J g^{-1}. This demonstrates that, over the cooling rate range of 1-10 °C min^{-1}, the extent to which PCL can crystallize does not vary significantly. The only difference is in the temperature range over which crystallization occurs which, as would be expected, decreases with faster cooling.

It is also relevant to mention here that PCL is a polymer that can crystallize by itself on storage at room temperature. This is made possible by the fact that, at room temperature, PCL is almost 100°C above its T_g and only 30-40°C below its T_m. Thus, room temperature is, in effect, an 'annealing' temperature for PCL at which the polymer's chain mobility enables further crystallization to occur. Hence, it is not uncommon for the % crystallinity of PCL, after cooling from the melt, to increase during storage.

Other important considerations in melt spinning, indeed in melt processing in general, are the polymer's thermal stability in the melt state and the width of its processing range. This is particularly relevant in the case of aliphatic polyesters which are susceptible to transesterification reactions in the melt. These are degradative reactions which lead to a reduction in the average molecular weight (by intramolecular transesterification) and/or a broadening of the molecular weight distribution (by intermolecular transesterification). Both have an effect on the properties of the final product. The extent to which these reactions occur depends mainly on the chemical environment of the ester group, the reaction temperature, and time, Generally, transesterification precedes the onset of actual weight loss by volatilization and so the TG curve for the PCL beads in Fig. 3.7 needs to be interpreted with caution. Whilst it may appear from the initial weight loss temperature of >250°C that PCL has a very wide melt processing range (cf., T_m = 60°C), in fact the processing range will be somewhat narrower than this suggests. Transesterification reactions may begin to occur at temperatures well below 200°C and so the melt spinning temperature should be kept as low as the melt viscosity and filament line stability allow.

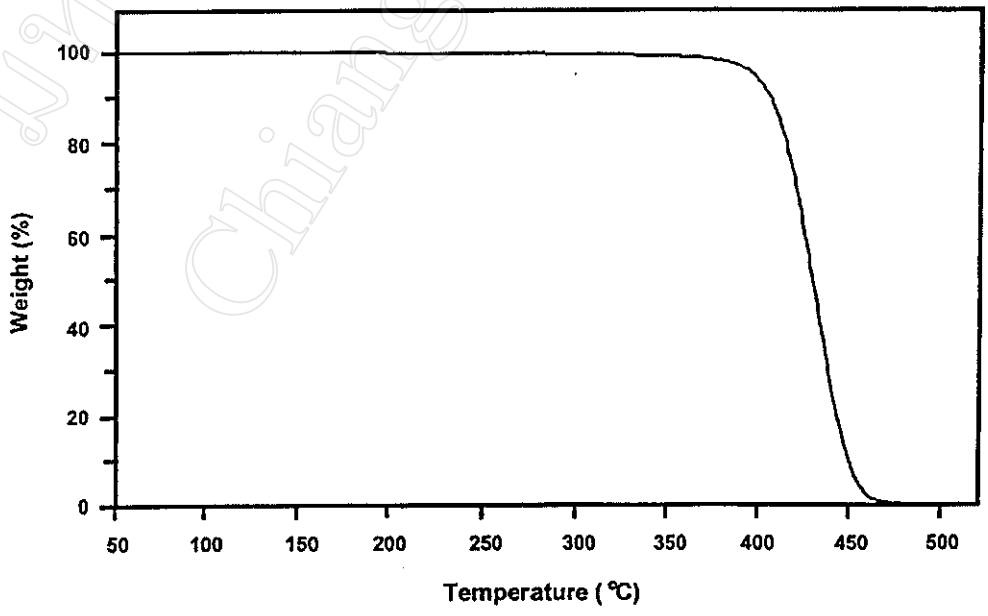

Fig. 3.7 TG curve showing the thermal decomposition (weight loss) range of the PCL beads. (Heating rate = 20°C min^{-1})

3.3.2.3 Melt Flow Properties

The melt rheology and, more specifically, the melt viscosity of a fibre-forming polymer is of critical importance in its melt spinning since it has profound effects on filament line stability and dimensional control. The temperature-dependence of the melt viscosity of the PCL used in this work is shown in Fig. 3.8 as a graph of melt flow index (MFI) against temperature at constant load (pressure). Measurements were made in accordance with ASTM Method D 1238 – 90b. It was found that the PCL could not be extruded smoothly at temperatures below 80°C (i.e., at temperatures less than 20°C above its melting range) due to too high a melt viscosity. Above 80°C, the polymer's MFI increases (i.e., melt viscosity decreases) with temperature, as would be expected.

Indeed, this melt viscosity-temperature dependence can be described mathematically. It has been found that, for polymers of relatively low molecular weight, low melt viscosity, and at melt temperatures which are more than 100°C above the polymer's T_g, as in the case of the PCL (T_g = -60°C) used here, the melt viscosity-temperature (η_{melt} – T) dependence shows close adherence to the Arrhenius-type equation:

$$\eta_{melt} = A \exp(E/RT) \qquad (3.4)$$

where A is a constant (pre-exponential coefficient), E is the activation energy for viscous flow and R is the universal gas constant. Thus, a graph of ln η_{melt} against 1/T yields a reasonable straight line of slope E/R which, for most polymers that satisfy the above criteria, usually extends over about a 50-150°C wide temperature range [54].

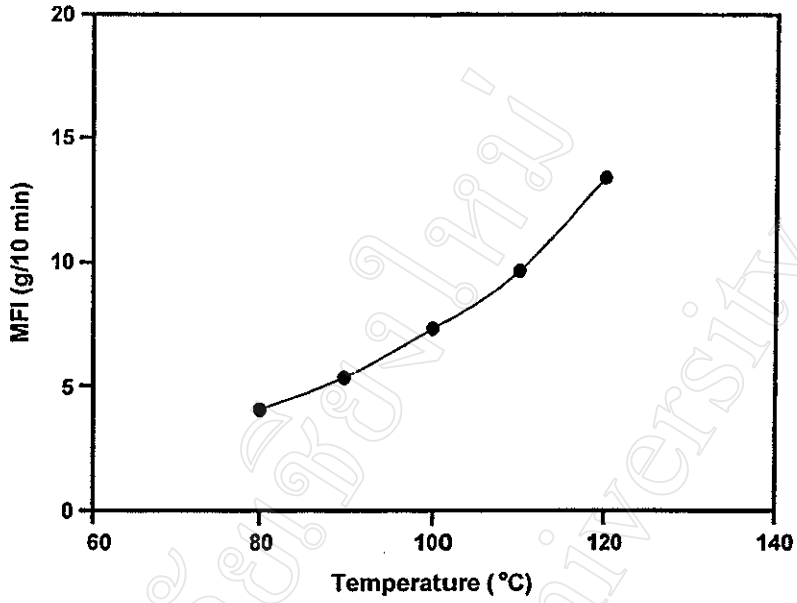

Fig. 3.8 Graph showing the variation in melt flow index (MFI) with temperature under constant load for the PCL beads. (Load = 2.16 kg, pressure ≈ 300 kPa)

3.4 Melt Spinning

3.4.1 Practical Considerations

One of the prime considerations in any melt spinning process is the melt spinning temperature. This is because the spinning temperature determines the melt viscosity which, together with the extrusion and take-up rates, determines the filament line stability. For the PCL used here, it was found that a spinning temperature of 85-90°C yielded fibres of optimum quality in terms of their smooth surface appearance and uniformity of diameter. At higher spinning temperatures of up to 120°C, the fibres obtained were still uniform in diameter but, as the melt viscosity decreased, the filament line started to show some initial signs of capillary instability.

As mentioned previously, PCL has a wide melt processing range due to its low melting point and high thermal stability. In such a case, it is preferable to choose a spinning temperature near the lower end of the range, usually around 20-40°C above the melting range. The higher the temperature, the more heat that needs to be dissipated from the extruded fibre as it cools. Hence, increasing the spinning temperature above the required minimum should only be considered if it is really necessary to lower the melt viscosity. In addition to the spinning temperature, the other main processing variables are the extrusion rate (ram speed), take-up rate, spinnerette diameter, and the vertical distance from the spinnerette to the cooling bath. Together, these variables control the as-spun fibre diameter at the macroscopic level and the molecular orientation and semi-crystalline morphology at the microscopic level.

3.4.2 Pre-Formed Rod Preparation

Prior to melt spinning, the PCL beads were first compressed into pre-formed cylindrical rods. This was done by warming the beads in the cylinder end-capped with a plain blanking plate under pressure from the ram. A temperature of 40-50°C was found to be suitable for this purpose, just enough for the beads to soften and stick together without appreciable melting. Melt spinning from rods gave fibres of more consistent quality than from beads and also reduced the tendency for void formation.

The various accessories which were used for this rod preparation are shown in Fig. 3.9. These accessories were used in conjunction with the small-scale melt spinning apparatus described in the previous chapter.

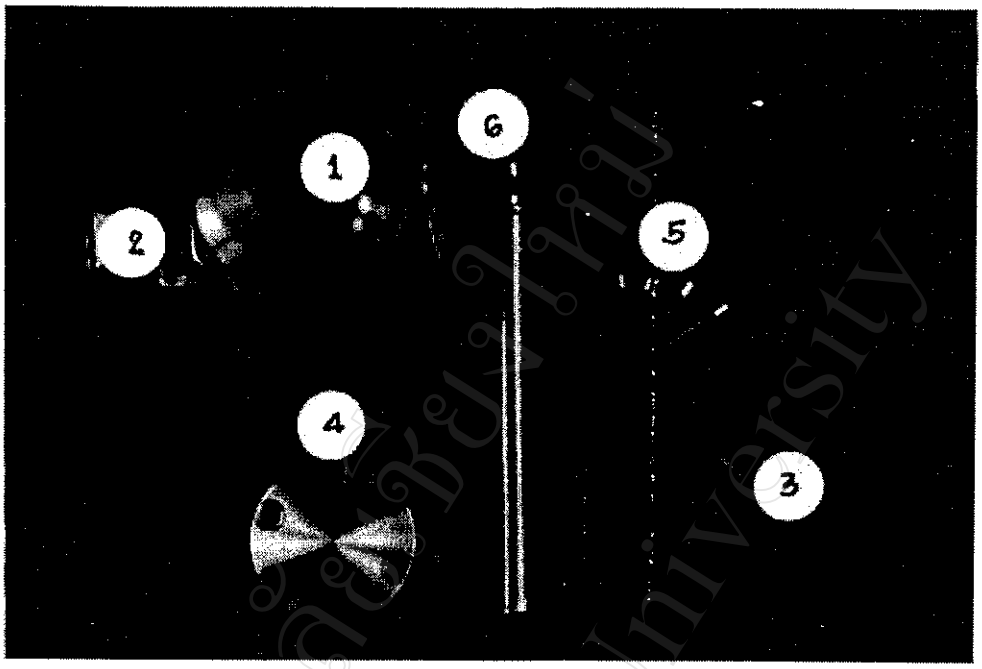

Fig. 3.9 The various accessories used in pre-formed rod preparation.

1. cylinder (inside diameter = 16 mm, length = 150 mm)
2. band heater
3. copper gasket
4. plain blanking plate
5. 20 mm cap screws
6. ram (piston)

The pre-forming cylinder with a full-length band heater clamped around it was assembled as shown if Fig. 3.10. The copper gasket and the plain blanking plate were then bolted to the base of the cylinder by means of 6 x 20 mm cap screws. These screws were lubricated with anti-seizure compound.

Fig. 3.10 The assembled pre-forming cylinder used for making PCL rods.

In a typical preparation, approximately 10-20g of the PCL beads, which had previously been dried in a vacuum oven at 40°C for 24 hours, were placed in the pre-forming cylinder. The cylinder assembly was placed in the extrusion unit, the heater plug connected and the thermocouple inserted into its hole. The beads were then compressed at a temperature of 40-50°C so that they softened, without actually melting, just enough to stick together in the shape of a cylindrical rod. On cooling and removing from the cylinder, the rod had a exterior with the outlines of the beads distorted but still discernable. Several rods were prepared in this way one after the other and then stored in a vacuum desiccator until required for use in fibre spinning.

3.4.3 Fibre Spinning

3.4.3.1 Set-up and Procedure

Following the pre-formed rod preparation, the cylinder assembly was modified for fibre spinning. This involved removing the full-length band heater and blanking plate, as shown in Figs. 3.9 and 3.10, and replacing them with the heating block, its own smaller band heater, and a spinnerette. A schematic diagrams of the heating block and spinnerette were shown in the previous chapter in Fig. 2.4 on page 32 and the complete assembly is photographed in Fig. 3.11 on the following page.

To commence fibre spinning, the cylinder assembly in Fig. 3.11 was placed in the control unit and the melt spinning apparatus arranged as shown previously in Figs. 2.1 and 2.2 (on pages 29 and 30). A pre-formed PCL rod, again pre-dried at 40°C in a vacuum oven for 24 hours, was carefully inserted into the extrusion cylinder and the ram (piston) placed in position. The rod was then heated up to the required melt spinning temperature and, when the temperature had reached equilibrium, the ram was lowered at the chosen speed to compress and extrude the molten PCL. As the extruded filament emerged from the spinnerette and cooled in contact with the cool room air, it was grasped with a pair of tweezers and led around two ceramic guides in the ice-water cooling bath. Finally, it was wound twice around a pair of take-up rollers before being collected on a bobbin, as shown in Fig. 2.1 on page 29. Since there were so many variables involved in this process, some of the less influential were kept constant. For example, the batch size (i.e., rod weight) and ice-water cooling bath temperature were kept constant throughout at 15-20 g and 5-10°C respectively. The effects of some of the more influential processing variables are now described in the following section.

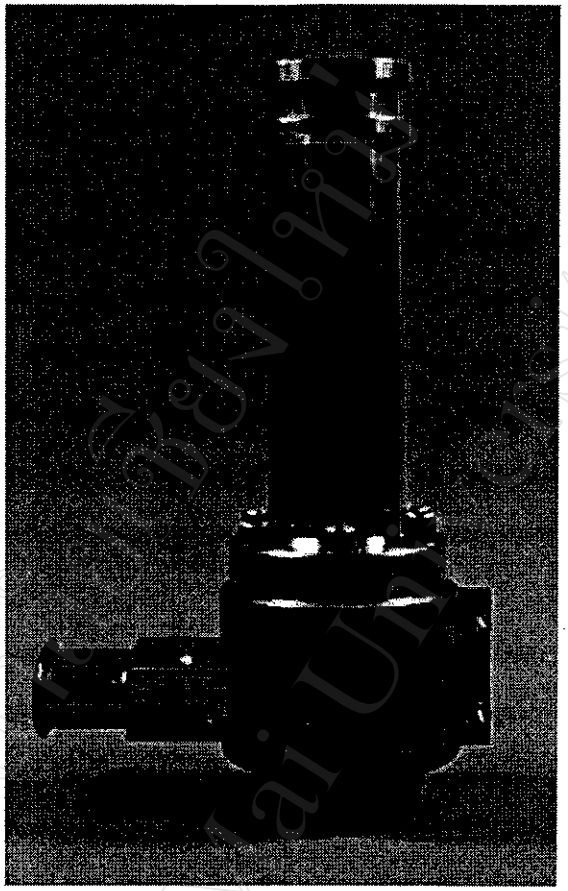

Fig. 3.11 The assembled extrusion cylinder ready for fibre spinning.
(For more detailed diagrams, see Fig. 2.4 on page 32.)

3.4.3.2 Effects of Processing Variables

(a) Melt Spinning Temperature

The effect of the melt spinning temperature on fibre diameter is shown in Table 3.2. Increasing the spinning temperature decreases the melt viscosity (according to the previous equation 3.4) which, in turn, facilitates melt flow through the heating block, stainless steel filter mesh and spinnerette. However, as explained in the previous chapter, increasing the spinning temperature above the necessary minimum for smooth extrusion and take-up is often counter-productive since (a) it can lead to capillary instability and (b) more heat needs to be dissipated from the extruded fibre as it cools.

From the melt spinning runs carried out here on the PCL rods, it was concluded that a spinning temperature of 85-90°C gave the best results on the basis of a smooth operation and uniform fibre diameter at the lowest possible temperature.

(b) Ram and Take-up Speeds

As would be expected, increasing the ram speed at constant take-up speed increases the fibre diameter while the reverse case decreases the fibre diameter. The results in Table 3.2 confirm this. When the ram speed is converted into an extrusion rate from the spinnerette, its ratio with the take-up rate gives the ***on-line draw ratio***, also sometimes referred to as the ***spin stretch ratio***.

$$\text{On-line draw ratio} = \frac{\text{take-up rate}}{\text{extrusion rate}} \qquad (3.5)$$

The extrusion rate can be calculated from the ram speed on the basis of volume displacement by assuming that the volume of the molten polymer inside the extrusion cylinder displaced by the piston equals the volume of the molten polymer exiting from the spinnerette hole. Therefore, if:

Extrusion volume (inside the extrusion cylinder) = $\pi r_1^2 h_1$

Extruded volume exiting from the spinnerette = $\pi r_2^2 h_2$

where $\pi r_1^2 h_1 = \pi r_2^2 h_2$

h_1 = rate of vertical displacement of the ram (i.e., ram speed)

h_2 = length of extruded fibre per unit time (i.e., extrusion rate)

r_1 = internal radius of the extrusion cylinder

r_2 = radius of the spinnerette hole

Table 3.2 Summary of the effects of some processing variables on the as-spun monofilament fibre diameter. (Spinnerette diameter= 2.0 mm, spinnerette to cooling bath air gap = 4.00 cm)

Spinning Temperature [a] (^{o}C)	Ram Speed [b] (mm/min)	Extrusion Rate [c] (m/min)	Take-up Rate [d] (m/min)	On-Line Draw Ratio [e]	Fibre Diameter [f] (mm)
85	2.0	0.12	0.60	5	0.91 ± 0.02
90	2.0	0.12	0.60	5	0.81 ± 0.02
100	2.0	0.12	0.60	5	0.80 ± 0.02
110	2.0	0.12	0.60	5	0.80 ± 0.02
120	2.0	0.12	0.60	5	0.79 ± 0.02
85	0.5	0.03	0.60	20	0.50 ± 0.02
85	1.0	0.06	0.60	10	0.66 ± 0.02
85	2.0	0.12	0.60	5	0.91 ± 0.02
85	2.0	0.12	0.60	5	0.91 ± 0.02
85	2.0	0.12	1.00	8.3	0.67 ± 0.02
85	2.0	0.12	2.00	16.7	0.49 ± 0.02

[a] as measured by the thermocouple, as shown in Fig. 2.4

[b] constant rate of descent of the ram, as shown in Fig. 2.4

[c] calculated from the ram speed via volume displacement

[d] wind-up speed on rollers of take-up unit, as shown in Fig. 2.1

[e] on-line draw ratio = take-up rate ÷ extrusion rate

[f] average of 50 readings taken with a digital micrometer

Therefore, to take an example from Table 3.2, for a ram speed (h_1) of 2 mm/min, a cylinder of internal radius (r_1) of 7.75 mm, and a spinnerette hole of radius (r_2) 1.0 mm, the calculated extrusion rate (h_2) is given by:

$$h_2 = \frac{r_1^2 h_1}{r_1^2} = \frac{(7.75)^2\, 2}{(1.0)^2} \text{ mm/min}$$

$$h_2 = 120 \text{ mm/min} = 0.12 \text{ m/min}$$

This extrusion rate of 0.12 m/min can now be compared with the corresponding take-up rate of, say, 0.60 m/min (in Table 3.2) to give the on-line draw ratio as:

$$\text{On-line draw ratio} = \frac{\text{take-up rate}}{\text{extrusion rate}} = \frac{0.60 \text{ m/min}}{0.12 \text{ m/min}} = 5$$

However, it should be emphasized here that these calculated values of the extrusion rate and the on-line draw ratio are only good approximations since they do not take into account effects such as melt compressibility, die swell, and volume contraction on cooling.

(c) Spinnerette Hole Size

Obviously, as the spinnerette hole size increases, the fibre diameter increases, although not necessarily in proportion. Indeed, the hole size is only one of a range of variables that determine the fibre diameter. The final fibre diameter on the bobbin is invariably less than the spinnerette hole size due to the combined effects of elongational flow and on-line drawing. A certain minimum amount of on-line drawing is necessary to take up any slack in the filament line and keep it taut as it passes around the guides and rollers.

In this work, a single-hole spinnerette of hole size 2.0 mm diameter was used as standard. When a smaller spinnerette of 1.0 mm diameter was used, the effect on fibre diameter at different ram speeds but constant take-up speed was as shown in Table 3.3. The results are consistent with the above remarks.

Table 3.3 Effect of spinnerette hole size on PCL fibre diameter at different ram speeds. (Temperature = 85°C, take-up speed = 0.60 m/min, spinnerette to cooling bath air gap = 4.00 cm)

Spinnerette Diameter (mm)	Ram Speed (mm/min)	On-line Draw Ratio	Fibre Diameter* (mm)
1.0	0.5	20	0.43 ± 0.02
1.0	1.0	10	0.63 ± 0.02
1.0	2.0	5	0.83 ± 0.02
2.0	0.5	20	0.50 ± 0.02
2.0	1.0	10	0.66 ± 0.02
2.0	2.0	5	0.91 ± 0.02

* average of 50 readings taken with a digital micrometer

(d) Spinnerette to Cooling Bath Air Gap

The vertical distance (air gap) between the spinnerette face and the cooling bath is known to have an effect on the fibre diameter. Generally, it is an inverse relationship since the greater the distance the more the cooling filament is likely to undergo thinning due to elongational flow under gravity. In this project, the standard air gap employed was 4.0 cm. This was the distance between the spinnerette face and the surface of the ice-water cooling bath.

The results in Table 3.4 show the effect of varying the air gap on the fibre diameter under the otherwise standard conditions of 85°C, 2.0 mm spinnerette, 2 mm/min ram speed and 0.6 m/min take-up speed. Interestingly, the results do not show the expected trend of decreasing fibre diameter with increasing air gap. Instead, the diameters are up and down with no discernable trend. A possible explanation

Table 3.4 Effect of air gap on PCL fibre diameter under otherwise constant conditions. (Temperature = 85°C, spinnerette diameter = 2.0 mm, ram speed = 2.0 mm/min, take-up speed = 0.6 m/min)

Air Gap (cm)	Fibre Diameter* (mm)
1.0	0.92 ± 0.01
2.0	0.95 ± 0.01
4.0	0.91 ± 0.02
5.0	0.85 ± 0.02
10.0	0.77 ± 0.03
15.0	0.69 ± 0.03

* average of 50 readings taken with a digital micrometer

for this is that, in fact, there is no trend to observe because PCL is such a fast crystallizing polymer that its semi-crystalline matrix gives the cooling filament dimensional stability against elongational thinning. The relatively small differences in fibre diameter in Table 3.4 are simply variations within the limits of experimental control.

(e) Effect of the Stainless Steel Wire Mesh

The stainless steel wire mesh was positioned at the bottom of the heating block at the entry to the spinnerette (Fig. 2.4, page 32). Its main function in this work was to shear the molten polymer so as to assist it to flow smoothly through the spinnerette.

However, because the mesh also represents a resistance to the melt flow, it is possible that it may cause a back pressure to build up inside the system which may, in turn, create a pressure drop across the mesh. It was of interest in this work to see if (a) the number of wire mesh discs and (b) the mesh size, both of which might influence the pressure profile, had any significant effect on the extruded fibre diameter.

The standard condition employed in this work was to use two wire mesh discs of mesh size 300 (i.e., 300 holes/cm^2). The higher the number, the finer the mesh. The results of experiments carried out using different numbers of discs and mesh sizes, under otherwise identical conditions, are given in Table 3.5. The results do not appear to indicate any definite trend as far as the fibre diameter is concerned. Thus, it must be concluded that the afore-mentioned pressure effects, if indeed they occur, do not significantly affect the melt flow through the system in this particular case. This could be because PCL has a relatively low melt viscosity which enables it to pass quite easily through the mesh. Consequently, the pressure profile within the system is not significantly altered by the presence of the mesh once the system has attained a 'steady state' of operation.

Table 3.5 Effect of stainless steel wire mesh on PCL fibre diameter under otherwise constant conditions. (Temperature = 85°C, spinnerette diameter = 2.0 mm, ram speed = 2.0 mm/min, take-up speed = 0.6 m/min)

Number of Discs	Mesh Size	Fibre Diameter* (mm)
0	-	0.89 ± 0.02
1	300	0.90± 0.02
2	300	0.91 ± 0.02
2	187	0.81 ± 0.03
2	150	0.85 ± 0.02
2	100	0.86 ± 0.03

* average of 50 readings taken with a digital micrometer

3.4.3.3 On-line Structural Development

In conclusion of this section on melt spinning, it is important to know how the dimensions (diameter) and morphology (% crystallinity) of the filament develop between emerging from the spinnerette and being wound up on the final take-up bobbin. This was studied here by taking samples at 4 different positions along the filament line, as shown in Fig. 3.12, and measuring their diameters and DSC heats of melting (∝ % crystallinity). These 4 positions were:

1. in the air gap just below the spinnerette
2. in the cooling bath between the 2 guides
3. on the pair of take-up rollers
4. on the final bobbin

The results in Table 3.6 show how the fibre diameter and % crystallinity develop on-line as the fibre cools and stretches. The results lead to 2 main conclusions:

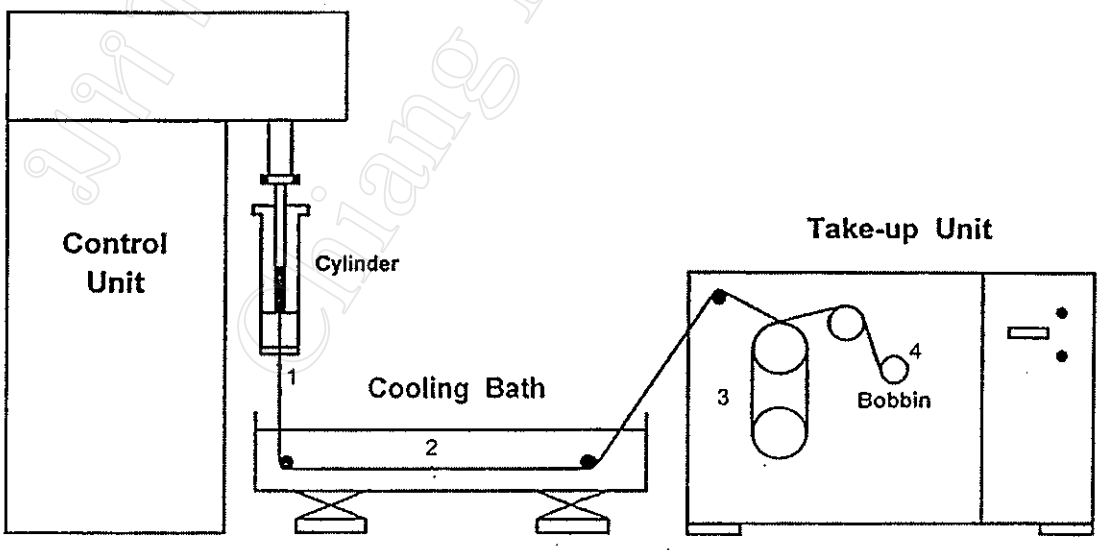

Fig. 3.12 Diagram showing the 4 positions along the filament line at which samples were taken for studying on-line structural development.

(1) The fibre's diameter is largely established by the time that it has completely solidified in the cooling bath. Further small decreases may take place as the fibre is stretched as it is wound up around the take-up rollers and bobbin.

(2) The fibre's % crystallinity also quickly reaches its near-maximum level once the fibre has solidified in the cooling bath. This is consistent with the previous DSC-based observations that PCL is a fast crystallizing polymer. The % crystallinity at position (1) in the air gap could not be measured because the fibre was still in the process of cooling at this position. The further increase in % crystallinity from 49% to 56% between the cooling bath and the bobbin is probably simply due to a completion of the cooling and solidification processes.

Table 3.6 Variations in PCL fibre diameter and % crystallinity along the filament line during melt spinning. (Temperature = 85°C, spinnerette diameter = 2.0 mm, ram speed = 2.0 mm/min, take-up speed = 0.6 m/min)

Filament Line Position (Fig. 3.12)	Fibre Diameter (mm)	Crystallinity* (%)
(1) air gap	2.09 ± 0.07	* *
(2) cooling bath	0.87 ± 0.03	49
(3) rollers	0.84 ± 0.02	56
(4) bobbin	0.83 ± 0.02	56

* determined from the DSC heat of melting, ΔH_m, followed by substitution into equation (3.3) on page 61

* * indeterminate (fibre still cooling)

3.5 Fibre Testing – Mechanical Properties

Finally, the mechanical properties of the as-spun fibres were examined by tensile testing. Testing was performed using a Lloyds LRX+ Universal Testing Machine

equipped with bollard-type grips and a 100 N load cell. A typical stress-strain curve is shown in Fig. 3.13(a). Even though the sample in Fig. 3.13(a) was over 50% crystalline (from its DSC curve), it was still a very weak fibre which could be stretched easily to over 20 times it original length without breaking. This is indicative that the spinning process introduced very little if any molecular orientation along the fibre axis.

However, when the same as-spun fibre was drawn at room temperature to off-line draw ratios of 5, 10, 15, 20 and 25 and then re-tested, the stress-strain curves in Figs. 3.13(b)-(f) show quite clearly the reinforcing effects of orienting the fibre's semi-crystalline morphology. This demonstrates that the combination of on-line and off-line processing variables controls not only the fibre diameter but also the chain orientation and mechanical properties. More detailed studies of the effects of off-line drawing temperature and rate on fibre morphology and properties should form the subject of further work.

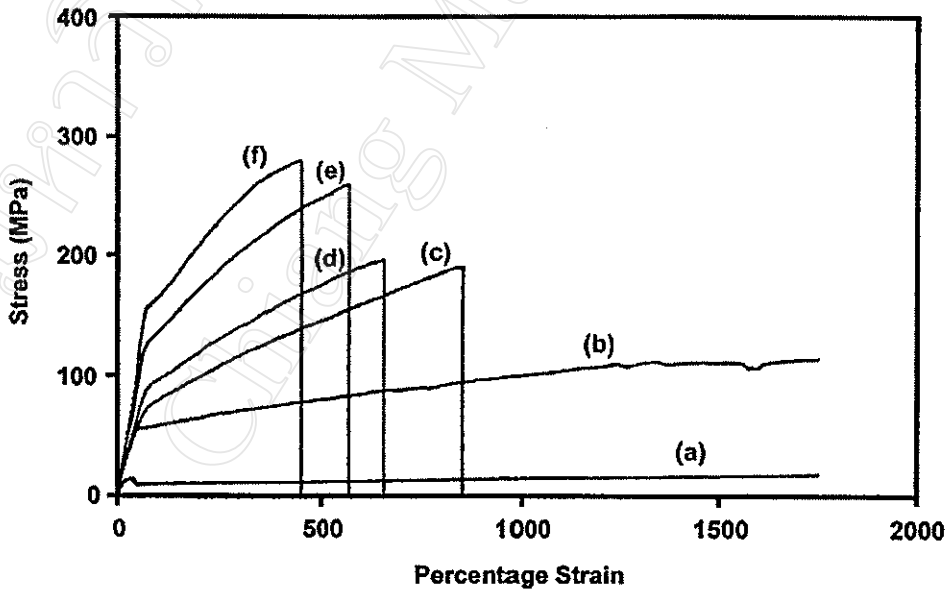

Fig. 3.13 Stress-strain curves of the PCL fibres showing the effects of increasing the off-line draw ratio (OffLDR) on tensile properties.

(a) as-spun fibre (b) OffLDR = 5 (c) OffLDR = 10

(d) OffLDR = 15 (e) OffLDR = 20 (f) OffLDR = 25

(initial gauge length = 40 mm, drawing rate = 20 mm min^{-1})

3.6 General Conclusions

The melt spinning process which has been described here is a simple batch-type discontinuous process for the production of monofilament fibres. It is suitable for small-scale experimental work, and even small-scale production, but not for the large-scale, high-speed production of commercial textile fibres. For speciality polymers which find use in high-value but low-volume applications, this type of small-scale operation is well-suited to its melt spinning into fibres. In such highly specialized applications, the polymer's semi-crystalline morphology often needs to be precisely controlled in order to meet specific property requirements. This is especially true in the case of biomedical fibres which need to have the appropriate balance of physical, mechanical and biological properties, all of which depend on filament size and morphology. In order to achieve this balance, the various factors which affect the polymer's spinnability and crystallizability need to be clearly understood. This has been the main focus of attention in this part of the work using PCL as a model polymer.

Another advantage of the small-scale batch-type process is that it allows the process as a whole to be divided up into separate stages, thereby increasing the degree of control over structure formation. For example, in the first stage, the emphasis can be placed on producing high-quality as-spun fibres of uniform diameter and smooth surface topography. Their % crystallinity and/or degree of molecular orientation are kept to a minimum during this initial stage. Then, in subsequent stages, the required matrix morphology can be gradually built into the fibres via a series of controlled off-line drawing and annealing steps, as the series of stress-strain curves in Fig. 3.13 clearly show.

Turning our attention now from the process to the polymer, the results presented in this chapter have revealed a number of interesting features of PCL spinnability which are important to note. For example, under a given set of conditions, the fibre diameters

obtained were consistently uniform (usually to within ± 0.02 mm) despite the fact that such slow spinning speeds were used. While slow speeds facilitate heat removal, they sometimes give rise to an oscillatory instability known as 'draw resonance', the cause of which can be traced back to the tensile stress to which the extruded fibre is subjected. However, draw resonance was not encountered here with PCL within the range of conditions studied, neither were cohesive or capillary fracture. The spinning dynamics were therefore deemed to be conducive to the establishment of a stable filament line.

Another important parameter in any fibre spinning process is the previously mentioned, ***on-line draw ratio***. Usually, in the case of a high melting point (T_m > 200°C) fibre such as poly(ethylene terephthalate), which cools rapidly towards its glassy state, on-line drawing can impart substantial molecular orientation and, in doing so, can induce crystallization in the as-spun fibre [5]. Some of these '*in situ*' microstructural changes are visualized in Fig. 3.14. However, in the case of PCL, on-line drawing merely stretches what is a highly extensible filament only just below its T_m range. The draw ratios previously reported in Table 3.2 therefore serve only to maintain filament line stability and control the fibre diameter. It is unlikely that they would have any significant effect on molecular orientation. In order to achieve this, separate off-line drawing at room temperature is required.

A further observation on the as-spun fibres, not apparent from the previous tables of results, is that they were all semi-crystalline. The DSC curve shown Fig. 3.5(b) is typical. The combination of PCL's very low T_g and facile crystallization makes it extremely difficult, if not impossible, to produce amorphous fibres. Indeed, the as-spun fibres obtained here were all over 50% crystalline, even without the added inducement of chain orientation. Moreover, when chain orientation was introduced through off-line drawing, the % crystallinity of the fibre did increase slightly but not very much, as seen from the similar ΔH_m values in Figs. 3.5(b) and 3.5(c). This evidence suggests that the kinetic and thermodynamic parameters associated with PCL's crystallizability from the

melt are such that its % crystallization is determined more by the polymer's own characteristic properties, such as its temperature transitions and molecular weight, rather than the processing conditions. In support of this view, a marked (inverse) dependence of % crystallinity on molecular weight has already been established for PCL [36].

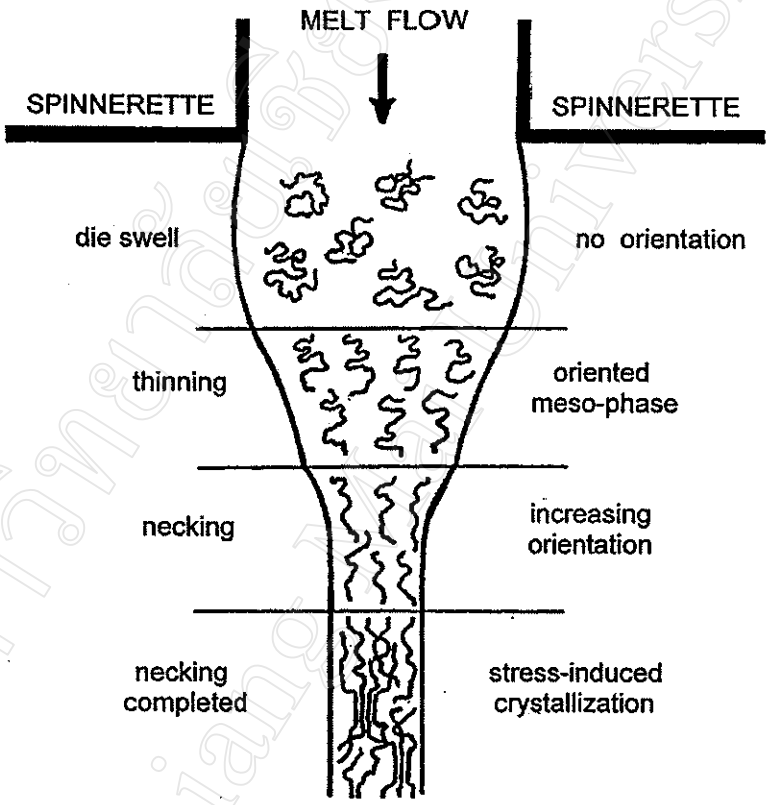

Fig. 3.14 Visualization of the sequence of molecular rearrangement processes which can occur during the melt spinning of a monofilament fibre.

Thus, PCL is a polymer of which the physico-chemical characteristics (chemical structure, transition temperatures) are such that they effectively pre-determine that the as-spun fibres will be semi-crystalline but largely unoriented. For certain fibre applications where tensile strength and modulus are not of critical importance, such as drug delivery systems and 3-D scaffolds for tissue growth, this type of morphology may

be acceptable as it is. However where strength and modulus are important, as in long-lasting absorbable sutures, an appropriate amount of chain orientation needs to be built in under controlled conditions.

The overriding conclusion from this work is that tailoring fibre properties to meet the demands of a specific application requires precise processing control. This, in turn, requires an insight into what the molecules are doing at each stage of the operation. Melt spinning is a complex multi-variate process. Some of the most obvious variables have been discussed here, others have not. For example, sample parameters such as molecular weight and batch size may also have significant effects. Furthermore, studies of the various stages of structure formation through techniques such as X-ray diffraction and birefringence measurements are clearly essential in order to verify the changes that are taking place. The valuable experience gained from this work with PCL, as described in this chapter, will be utilized in Chapter 5 when the fibre processing and testing of the synthesized co- and terpolymers will be described.